





Communication

Utilizing Optical Coherence Tomography to Estimate Ablation Depth on Intraocular Lenses (IOLs) Under Femtosecond Laser Ablation

Georgios Ninos ¹, Constantinos Bacharis ¹, Virgilijus Vaičaitis ², Ona Balachninaite ²
and Nikolaos Merlemis ^{3,*}

¹ Sector of Optics and Optometry, Laboratory of Optical Metrology, Department of Biomedical Sciences, University of West Attica, Ag. Spyridonos Street, 12243 Athens, Greece; gninos@uniwa.gr (G.N.); kbacharis@uniwa.gr (C.B.)

² Laser Research Center, Vilnius University, Sauletekio 10, 10223 Vilnius, Lithuania; virgilijus.vaicaitis@ff.vu.lt (V.V.); ona.balachninaite@ff.vu.lt (O.B.)

³ Department of Surveying and Geoinformatics Engineering, University of West Attica, Ag. Spyridonos Street, 12243 Athens, Greece

* Correspondence: merlemis@uniwa.gr

Abstract

Intraocular lens (IOL) implantation is currently the most effective method for restoring vision following cataract surgery and is also used in cases of high myopia or hyperopia. However, IOL implantation eliminates accommodation, forcing patients to choose between corrected distance vision, requiring reading glasses for near tasks, or near vision supplemented by distance correction with spectacles. This limitation underscores the need for fully customized, patient-specific IOLs. To address this challenge, we performed femtosecond laser ablation experiments on polymethyl methacrylate (PMMA) IOLs using 200 fs pulses at 513 nm to investigate controlled surface modification. Laser-induced surface structuring offers a pathway to inscribe micron-scale patterns, including apodized features, in transparent polymers. To our knowledge, this is the first demonstration of femtosecond laser irradiation at 513 nm applied to IOL surfaces. Furthermore, this study is the first to combine scanning electron microscopy (SEM) and optical coherence tomography (OCT) as detection technologies to analyze and quantify ablation morphology and depth. The formation of smooth craters with minimal surrounding thermal damage highlights the potential of femtosecond laser processing as a promising tool for the development of customized, patient-tailored intraocular lenses.

Keywords: intraocular lenses; laser ablation; femtosecond pulses; visible laser wavelength; optical coherence tomography



Received: 12 September 2025

Revised: 24 October 2025

Accepted: 31 October 2025

Published: 2 November 2025

Citation: Ninos, G.; Bacharis, C.; Vaičaitis, V.; Balachninaite, O.; Merlemis, N. Utilizing Optical Coherence Tomography to Estimate Ablation Depth on Intraocular Lenses (IOLs) Under Femtosecond Laser Ablation. *Photonics* **2025**, *12*, 1082. <https://doi.org/10.3390/photonics12111082>

Copyright: © 2025 by the authors. Licensee MDPI, Basel, Switzerland. This article is an open access article distributed under the terms and conditions of the Creative Commons Attribution (CC BY) license (<https://creativecommons.org/licenses/by/4.0/>).

1. Introduction

The human visual system is complex, consisting of the cornea, the crystalline lens, and the retina. Over time, the natural lens may develop opacities (cataracts), impairing its ability to focus light onto the retina and ultimately leading to vision loss [1]. Intraocular lenses (IOLs) are currently the most effective solution for restoring vision after cataract surgery and are also used in cases of high myopia, hyperopia, or presbyopia. Compared with corneal refractive surgery using excimer lasers, phakic IOLs for the treatment of high myopia can offer superior predictability and optical quality [2–4]. IOLs are implanted into the eye through small incisions to replace the natural lens. However, once the crystalline

lens is replaced, accommodation is lost. Patients must then choose whether to have their distance vision corrected with the IOL, requiring reading glasses for near tasks, or select an IOL power that provides some near vision and use spectacles for distance correction.

The earliest IOLs were made of polymethyl methacrylate (PMMA) and incorporated ultraviolet-blocking chromophores. Modern IOLs are fabricated from more flexible materials, such as silicone or hydrophobic acrylics, which allow folding and insertion through smaller incisions. Various IOL designs exist, including monofocal, toric, multifocal, accommodating, and aspheric types (Figure 1). Toric IOLs, in particular, have been widely adopted for correcting astigmatism, including in keratoconus and other corneal irregularities [5,6], and recent lenses have achieved improved rotational stability and higher spectacle independence. Some patients also adopt a monovision strategy, with one eye corrected for distance and the other for near vision.

To restore functional vision at multiple distances, multifocal IOLs were introduced. These lenses employ either refractive or diffractive designs, incorporating zones or steps that distribute light to near and far focal points [7–10]. A refinement of diffractive designs is apodization, where the diffractive step heights or transmission profile gradually decrease from the center toward the periphery. This approach smooths the transition between focal zones, reducing light scatter and halos while enhancing contrast sensitivity across lighting conditions.

Recently, laser ablation has been investigated as a method for post-implantation customization of IOLs. In PMMA, excimer laser irradiation produces microcraters whose morphology reflects complex nonlinear processes [11,12]. By selectively removing thin layers of material, pulsed lasers, from nanosecond (ns) to femtosecond (fs) pulse durations, can alter surface curvature and refractive properties, thereby fine-tuning optical power or correcting residual refractive errors after cataract surgery. Femtosecond pulses are especially attractive, since their ultrashort duration (<300 fs) minimizes thermal diffusion, enabling precise energy confinement and micro-structuring of transparent polymers [13]. The physical ablation mechanism in ultrashort pulses is inherently nonlinear, involving multiphoton ionization and plasma formation, followed by rapid expansion and shock-wave generation and subsequent plasma-mediated ablation. At sufficiently high intensities, nonlinear mechanisms such as multiphoton absorption dominate, allowing significant energy deposition even in materials transparent at the laser wavelength [14]. This leads to localized ionization, plasma generation, and shockwave dynamics, resulting in either surface micro-craters or refractive index modifications within the bulk material [15]. Material properties such as bandgap, thermal conductivity, and elasticity strongly influence the ablation threshold and morphology of the laser-processed region.

Experimental studies have explored a broad spectral range (193–1064 nm) and pulse durations spanning ns to fs, as well as continuous-wave lasers at visible wavelengths (e.g., 405 nm) for modifying PMMA and acrylic IOLs [16–19]. However, the morphological quality of the ablation craters has often remained suboptimal, especially in the case of longer pulse durations.

From a physics perspective, this capability to induce controlled modifications enables the engineering of customized optical functions in implanted IOLs. For instance, by designing the spatial distribution of laser-induced microstructures, gradient-index (GRIN) profiles could in principle be inscribed in micro-lenses [20], optimizing light propagation and minimizing aberrations. Femtosecond laser processing thus provides a powerful platform for patient-specific optical corrections [21]. For accurate prediction of ablation outcomes, mathematical models relating ablation rate to laser intensity must be adapted to each polymer system. Imaging tools such as scanning electron microscopy (SEM) and

atomic force microscopy (AFM) are critical for evaluating structural modifications, crater depth, and subsurface changes [16,22].

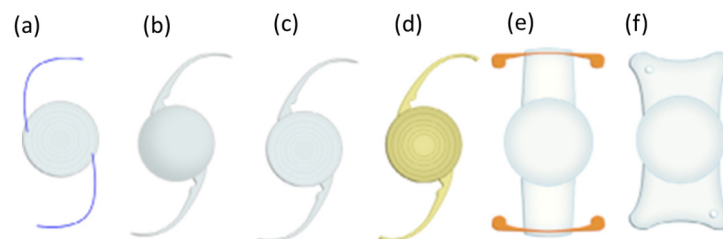


Figure 1. Representative examples of various commercial intraocular lenses (IOLs) and their haptics: (a–c) show multifocal designs; (d) is yellow due to its UV filter; (e) is an “accommodating” type and (f) is aspheric [18]. These images are included for illustration of general IOL geometries and do not correspond to the specific models used in the experiments of this study.

The aim of this study is to demonstrate, as a proof of principle, that femtosecond laser ablation can produce controlled and localized modifications on IOL surfaces, which may be linked to changes in refractive power and light transmission. These modifications include precise crater formation and possible subsurface refractive index changes. Unlike conventional manufacturing processes, femtosecond laser irradiation offers the possibility of post-fabrication adjustment of IOL properties. The use of 513 nm femtosecond pulses is particularly advantageous, as the short pulse duration and operation in the green spectral region minimize thermal effects and prevent carbonization, ensuring clean and precise modifications. PMMA IOLs were selected for this initial study because, despite their reduced use compared to acrylic lenses, they still represent a clinically relevant material and serve as a well-characterized model system suitable for controlled testing of the technique. The resulting modifications were analyzed using SEM for surface morphology and Optical Coherence Tomography (OCT) for depth profiling. We propose that OCT, complementary to SEM, provides accurate subsurface characterization of structural changes. Our findings suggest that femtosecond laser irradiation at this wavelength is a promising approach for post-manufacturing customization of PMMA IOLs, enabling patient-specific adaptations in refractive power. Such controlled surface modifications could, in principle, be further engineered to fine-tune the optical path and balance distance and near vision performance, although this lies beyond the scope of the present proof-of-concept study.

2. Materials and Methods

A simplified schematic of the experimental setup is shown in Figure 2. The laser source was a PHAROS femtosecond laser system (Light Conversion, Vilnius, Lithuania), emitting 200 fs pulses at a central wavelength of 513 nm (second harmonic). The experiments were conducted at the Laser Research Center of Vilnius University (VULRC). The maximum average output power was 528 mW, with a maximum repetition rate of 6 kHz. The beam diameter prior to focusing was 4.5 mm (measured at $1/e^2$ of the maximum intensity). No additional collimation optics were used prior to the focusing lens, since the output beams of the PHAROS femtosecond laser (fundamental and second harmonic) were already well collimated ($M^2 < 1.3$). The IOL samples were made of PMMA and had nominal powers of +24.5 dpt and +25.5 dpt (Hanita Lenses, model BAL-15, Kibbutz Hanita, Israel). During the experiments, the pulse energy and corresponding peak intensity were systematically varied to produce ablation spots of different sizes and morphologies.

The ablation spots produced on the IOLs were characterized using two complementary techniques. Structural and morphological features resulting from the ablation process

were examined using a scanning electron microscope (SEM, JEOL JSM-6510LV, JEOL, Tokyo, Japan).

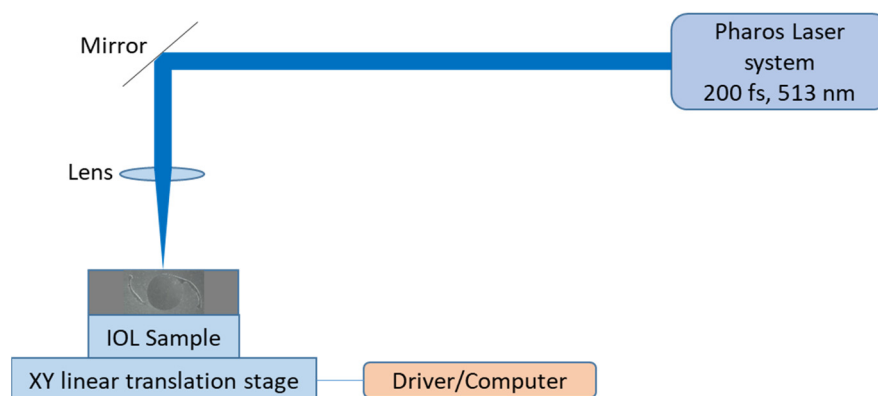


Figure 2. Simplified schematic of the experimental setup. The laser beam is focused on the sample by a 15 mm focal-length lens.

OCT is an imaging technique that acquires high-resolution cross-sectional images of scattering media by exploiting low-coherence interferometry. A broadband light source is split into two paths (reference and sample beams), similar to those in a Michelson-Morley interferometer. Light backscattered from different depths in the sample recombines with the reference beam to generate interference only when the optical path lengths match within the coherence length. From these interference signals, depth-resolved reflectivity profiles (A-scans) are constructed and subsequently assembled into cross-sectional (B-scan) images. Its real-time imaging capability and non-invasiveness make it an essential tool in ophthalmology and biomedical imaging research. In this study, OCT was specifically used to quantify the depth of ablation craters, to the best of our knowledge for the first time.

Our OCT system (Optovue RTVue Avanti XR, Optovue Inc., Fremont, CA, USA) provides an axial optical resolution of 5 μm and a transverse (lateral) resolution of 15 μm . It employs an 840 nm diode laser with a high scan speed of 70,000 A-scans per second and offers widefield imaging up to 12 mm in width. The OCT measurements were carried out at the Laboratory of Optical Metrology, Sector of Optics and Optometry, Department of Biomedical Sciences, University of West Attica. For imaging, the IOL samples were mounted on a kinematic optical holder to ensure accurate alignment and collimation with the OCT system (Figure 3). The IOL samples were further stabilized by mechanically fixing the haptics, the peripheral extensions of the IOLs that secure their position inside the eye, onto a polyurethane support.

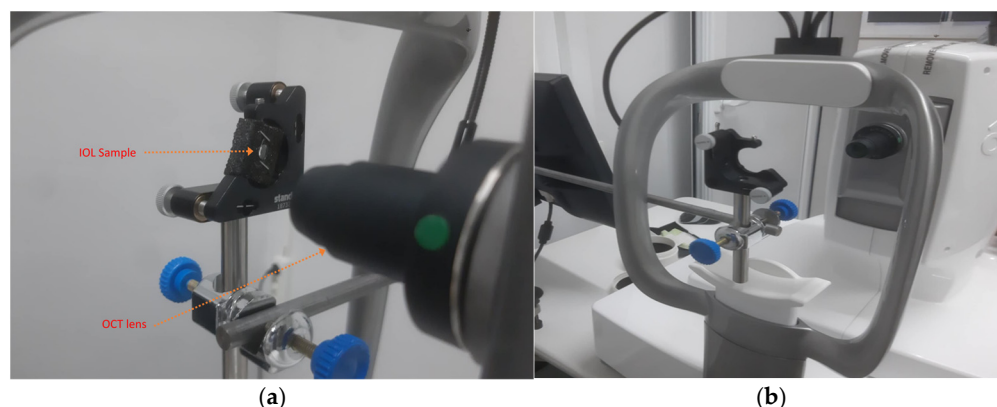


Figure 3. OCT experimental setup: (a) An IOL sample fixed in front of OCT objective lens, (b) Actual image of OCT Optovue RTVueAvanti XR.

3. Results

The experimental investigation focused on the surface modification of PMMA IOL samples under fs laser irradiation and under varying pulse energy and repetition rate conditions. The primary objective was to assess whether controlled and reproducible ablation features could be generated without compromising the optical quality of the lens. We present representative images of three ablated samples. Using 200 fs laser pulses at 513 nm (second harmonic), we observed the formation of well-defined microcraters on the lens surface. These craters displayed smooth and well-contoured edges, with no evidence of internal cracking or debris, an outcome that is essential for preserving the optical integrity of the intraocular lens (Figures 4–6).

A quantitative analysis of the ablation process was carried out by plotting the maximum crater depth as a function of the number of successive pulses delivered to the sample (Figure 7). For this measurement, the pulse energy was fixed at 88 μJ . The maximum depth corresponds to the mean value of crater depths obtained from multiple ablation sites created under identical irradiation conditions. The resulting curve shows a nonlinear dependence of depth on pulse count, indicating cumulative energy deposition and a tendency toward ablation saturation beyond a certain threshold.

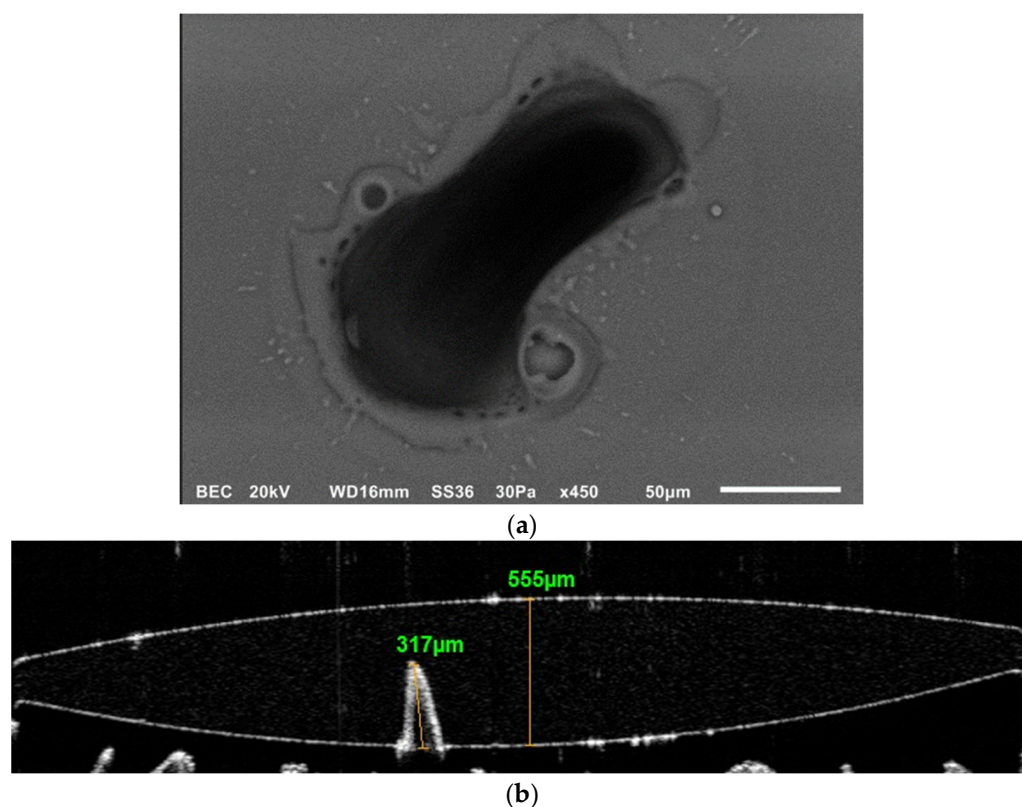


Figure 4. First IOL sample. Laser power was 528 mW, repetition rate was 6 kHz, 500 pulses were delivered on the sample. (a) SEM image of laser ablated spot; (b) OCT images of the measurements of both IOL thickness and the ablation depth. The IOL was positioned perpendicularly to the OCT lens axis; the lower part of the OCT image corresponds to the supporting polyurethane substrate. The ablation depth was determined from the OCT images using the system's proprietary analysis software.

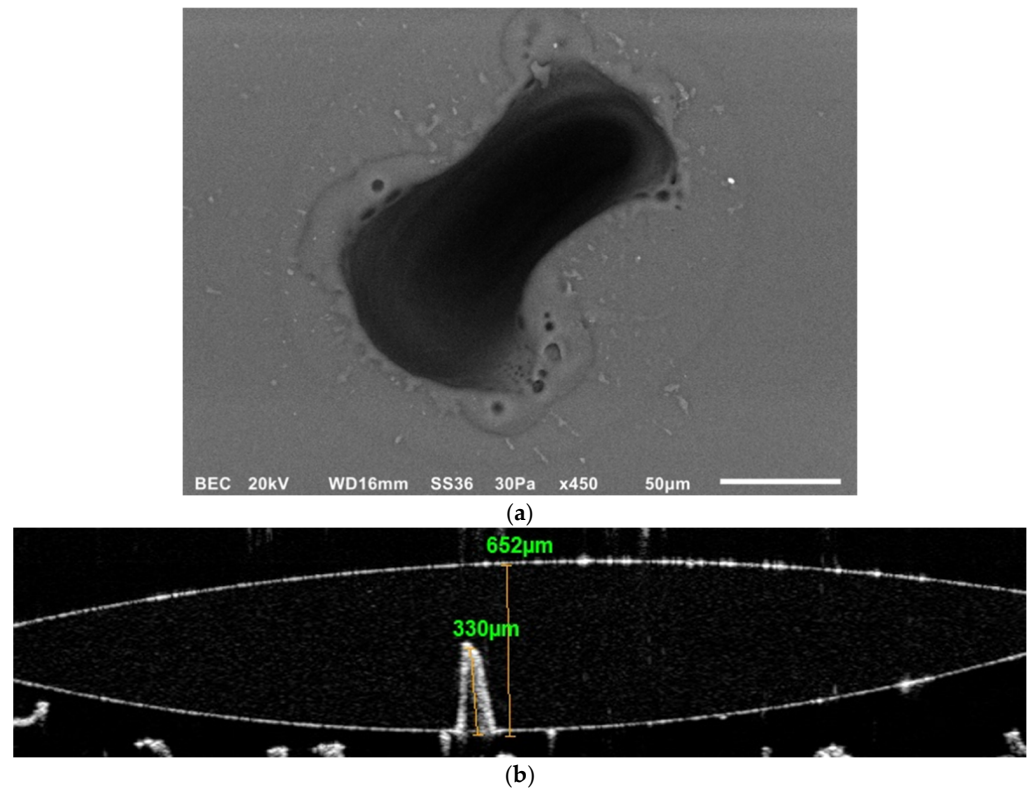


Figure 5. Second IOL sample. Laser power was 528 mW, repetition rate was 6 kHz, 500 pulses were delivered on the sample. (a) SEM image of laser ablated spot; (b) OCT images of the measurements of both IOL thickness and the ablation depth.

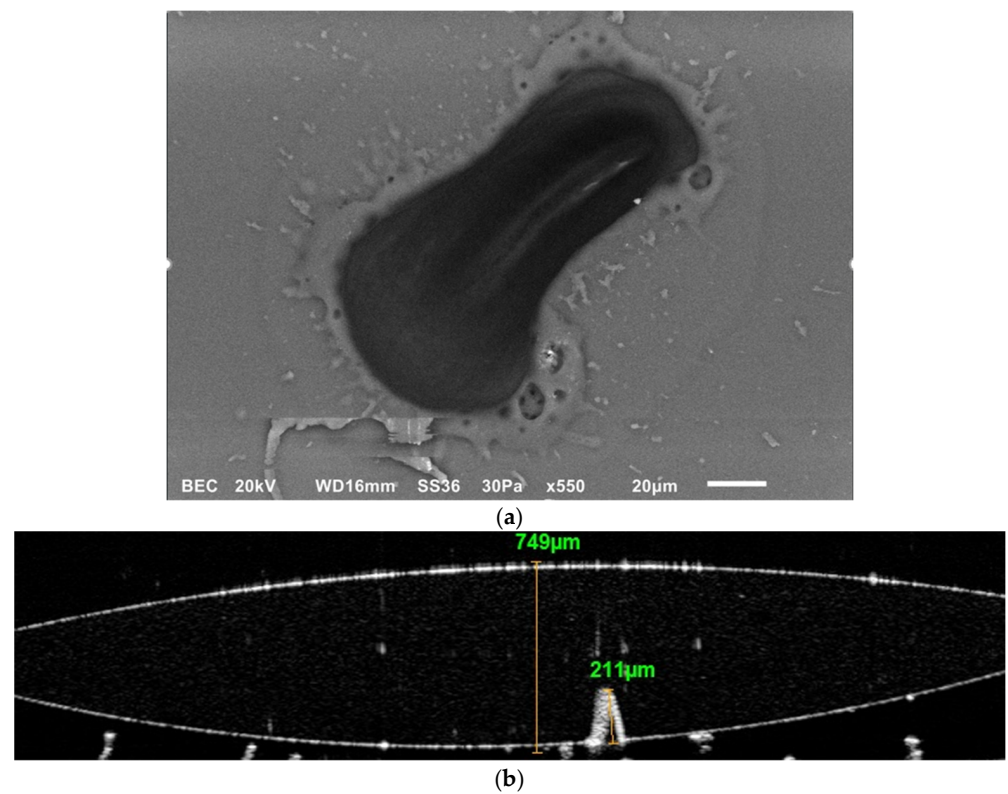


Figure 6. Third IOL sample. Laser power was 528 mW, repetition rate was 6 kHz, 200 pulses were delivered on the sample. (a) SEM image of laser ablated spot; (b) OCT images of the measurements of both IOL thickness and the ablation depth.

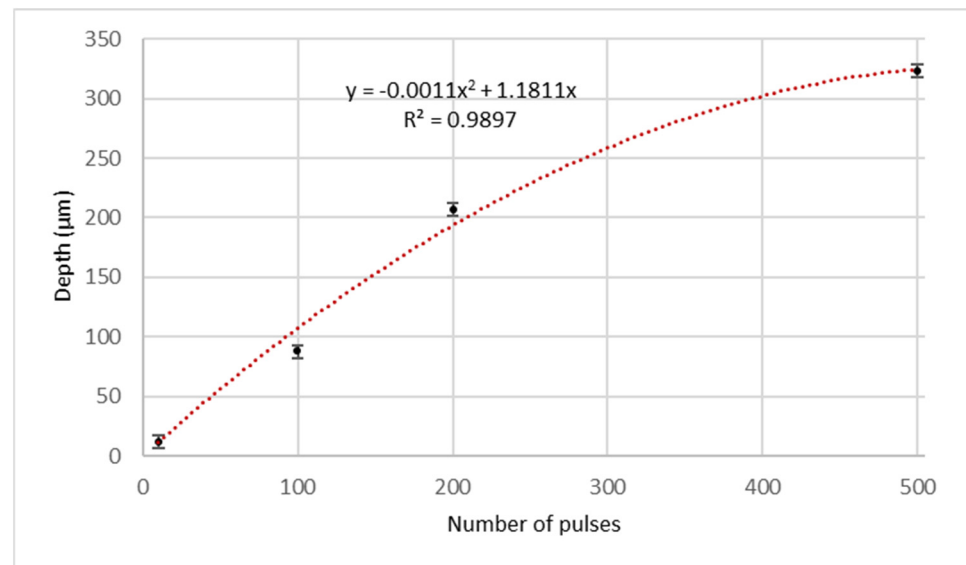


Figure 7. Plot of the maximum ablation depth versus the number of subsequent pulsed hitting the sample. The pulse energy was 88 μJ . The maximum ablation depth is the mean value of the measured depth for the ablation spots created under the same number of pulses. The ablation depth was determined from the OCT images using the system's proprietary analysis software. Error bars on the y-axis correspond to the resolution of the OCT system used.

The use of SEM enabled high-resolution visualization of surface features, confirming the absence of microfractures and the uniformity of crater geometry. OCT provided complementary subsurface profiling, revealing the depth and shape of the modifications with micron-level precision. These results demonstrate that femtosecond laser pulses at 513 nm can induce controlled and reproducible structural changes in PMMA IOLs. Moreover, the smoothness of the ablated structures suggests that such modifications could be harnessed for custom refractive tuning.

A further series of experiments was conducted using a motorized translation stage to move the samples at constant velocities, while the laser operated at fixed pulse energy and repetition rate. This setup allowed the relationship between translation scanning speed and the morphological characteristics of the inscribed ablation tracks to be systematically investigated. Using femtosecond pulses at a repetition rate of 6 kHz and a reduced average power of 75 mW, the samples were translated at scanning speeds of 50 $\mu\text{m/s}$, 100 $\mu\text{m/s}$, two measurements at 200 $\mu\text{m/s}$, 250 $\mu\text{m/s}$, and 300 $\mu\text{m/s}$. The resulting ablation tracks, along with the corresponding IOL sample, are shown in Figure 8. OCT analysis provided depth profiling of the tracks, with maximum depths measured at the deepest points along each path. The track widths ranged from 85 μm to 151 μm , while the IOL thickness was approximately 741 μm . As expected, lower scanning speeds resulted in longer beam dwell times on the material surface, leading to the delivery of a greater number of pulses per unit length. Consequently, an inverse relationship between scanning speed and ablation depth was observed: slower scanning speeds produced deeper and wider tracks, whereas faster speeds yielded shallower and narrower features.

The combined diagram in Figure 9, which includes the experimental data along with both quadratic and linear fits, provides a clear visualization of the relationship between scanning speed and ablation depth. The data points confirm a consistent decrease in ablation depth with increasing scanning speed, while the quadratic fit more accurately represents the nonlinear character of the interaction than the linear model. This analysis underscores the potential for developing predictive models in femtosecond laser microma-

chining and offers valuable guidance for optimizing laser parameters in the customized fabrication and post-processing of intraocular lenses.

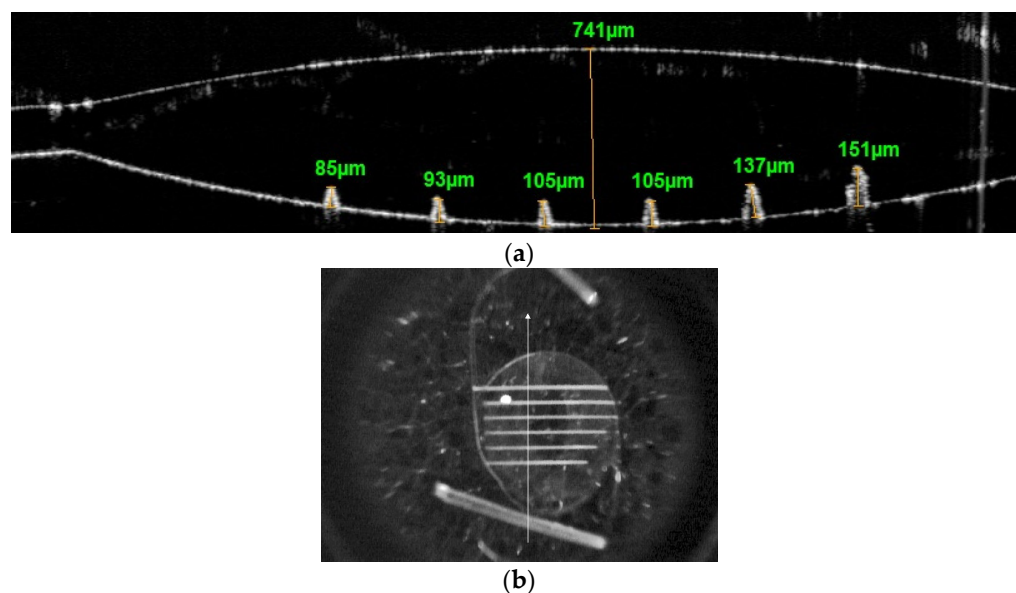


Figure 8. Influence of scanning speed on Ablation Depth; (a) OCT measurements for repetition rate 6 kHz, average power of 75 mW. Samples were moved at varying scanning speeds (from right to left): 50 $\mu\text{m/s}$, 100 $\mu\text{m/s}$, 200 $\mu\text{m/s}$, 200 $\mu\text{m/s}$, 250 $\mu\text{m/s}$, and 300 $\mu\text{m/s}$. The depths shown are the maximum depth of each ablation line (b) Actual image of the laser ablated IOL sample. The vertical line shows the sample section measured by the OCT scan.

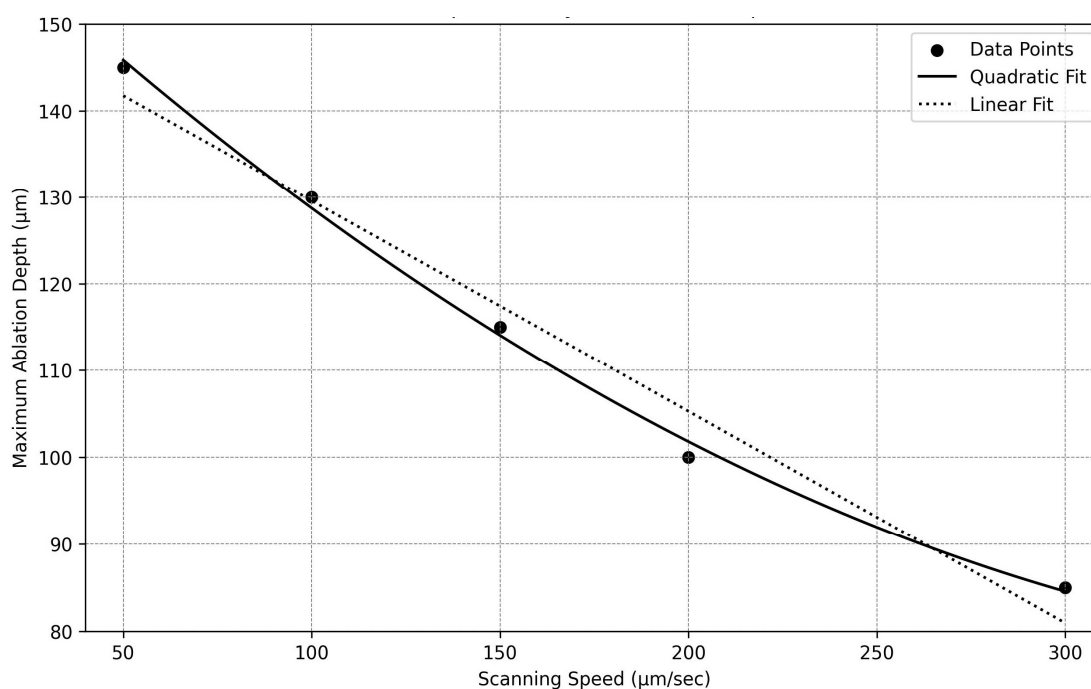


Figure 9. Relationship between scanning speed and maximum ablation depth in PMMA intraocular lenses. The plot includes experimental data points (dots), a best fit quadratic curve (dotted line), and a best fit linear regression line (solid line), illustrating the decreasing trend in ablation depth with increasing scanning speed.

The observed nonlinear dependence of ablation depth on scanning speed can be attributed to cumulative multi-pulse effects within the PMMA sample. At slower scanning speeds, the increased number of pulses delivered to a given location promotes energy

accumulation, which effectively lowers the ablation threshold, a phenomenon commonly referred to as the incubation effect. This effect, together with localized heating and nonlinear absorption (e.g., multiphoton ionization), results in disproportionately deeper and wider ablation tracks than predicted by a purely linear energy-deposition model. At higher scanning speeds, reduced pulse overlap limits cumulative energy deposition, yielding shallower, near-threshold features. These observations are consistent with previous reports on femtosecond laser micromachining of polymers, including PMMA [23,24].

4. Discussion

The interaction of 200 fs laser pulses at 513 nm with PMMA at the radiation energies employed in this study involves several nonlinear optical and thermally mediated processes, owing to the ultrashort pulse duration and the electronic structure of the material. PMMA has a bandgap of approximately 4–5 eV, considerably higher than the photon energy at 513 nm (2.42 eV), which makes single-photon absorption impossible. Under high peak intensities, however, nonlinear absorption becomes significant: two-photon absorption (2PA) or three-photon absorption (3PA) can excite electrons across the bandgap, while further intensity increases enable multiphoton ionization [25–29].

At sufficiently high intensities (typically in the TW/cm² regime), these multiphoton events can be accompanied by avalanche ionization, producing electron–ion plasmas (optical breakdown). Plasma formation in turn drives localized material modification, ablation, and, if uncontrolled, structural damage in PMMA. In the present experiments, the 200 fs pulses deposited energy faster than it could dissipate via thermal diffusion (ps–ns timescales), thereby restricting heat flow and limiting surrounding material modification. This regime favors the generation of smooth craters with sub-micron precision and minimal thermal cracking. No significant carbonization was observed in our experiments, which is consistent with the use of femtosecond pulses. Carbonization is typically associated with thermal effects that become more pronounced for longer pulse durations (ns or ps), where heat diffusion leads to collateral damage. In femtosecond ablation, the ultrashort pulse duration confines energy deposition within the optical penetration depth and minimizes heat transfer to the surrounding material. Furthermore, the choice of 513 nm (green) radiation also contributes to this outcome, as carbonization has been reported in the red region of the visible spectrum even under femtosecond excitation [13,16]. Thus, the combination of ultrashort pulse duration with operation in the green spectral region likely explains the absence of noticeable carbonization in our results. This finding highlights an additional advantage of visible femtosecond irradiation over longer-wavelength infrared lasers for precise micro-structuring of polymeric materials.

The relatively low thermal conductivity of PMMA nonetheless makes it susceptible to melting, vaporization, or decomposition at elevated fluences. Furthermore, PMMA exhibits a nonlinear refractive index on the order of $\Delta n \approx 10^{-3}$ – 10^{-2} , comparable to silica waveguides. At sufficiently high peak intensities, self-focusing effects may occur, which in turn can lead to filamentation or distortions in beam propagation. Depending on the fluence and focusing conditions, femtosecond pulses can induce permanent structural modifications in the polymer matrix, including densification or chain scission, enabling the inscription of waveguides or gratings within the bulk material [29–32].

In our study, under the specific conditions employed (200 fs, 513 nm, 6 kHz repetition rate), the dominant mechanisms in PMMA appear to be nonlinear absorption (2PA/3PA), plasma formation, and localized structural modification, with minimal surrounding thermal damage. This processing regime enables high-precision micromachining suitable for photonic device fabrication.

Experimentally, we observed that increasing the number of pulses within the investigated range led to a slightly non-linear increase in crater depth, while crater quality remained consistent, with smooth edges and minimal evidence of microcracks or thermal degradation. These findings suggest that femtosecond laser irradiation at 513 nm, under the pulse energies tested here, represents a promising technique for the post-manufacturing customization of PMMA IOLs. By focusing the laser within the interior of the IOL, controlled refractive index changes can be introduced, providing a potential pathway for post-manufacturing customization of IOLs through tailored light propagation [33]. Such an approach could enable patient-specific modifications in refractive power, while preserving the bulk integrity of the implanted lens.

5. Conclusions

The interaction of femtosecond laser pulses with PMMA intraocular lenses demonstrates significant potential for ophthalmic applications, particularly for precision micromachining and customized lens modification. This study showed that femtosecond irradiation at 513 nm can induce controlled structural changes on the surface of PMMA with minimal surrounding thermal damage, owing to the ultrashort pulse duration, the specific wavelength in the green spectral region, and high peak intensity. These findings support the feasibility of using femtosecond lasers in this spectral range for precise intraocular lens adjustments, enabling patient-specific refractive corrections or the inscription of functional surface features, either during manufacturing or as post-fabrication customization.

Further work is required, particularly with shorter wavelengths in the blue-UV range, to investigate the stability of subsurface and surface modifications under varying focusing conditions, both at the surface and within the lens interior, as well as long-term biocompatibility and the effects of repeated or high-energy exposures. Overall, the present results establish a proof of concept for femtosecond laser processing of IOLs combined with OCT metrology and highlight this dual-approach as a promising route toward the next generation of high-precision, patient-tailored intraocular lenses.

Author Contributions: Conceptualization, G.N., C.B. and N.M.; methodology, G.N., C.B. and N.M.; experiments, G.N., C.B., N.M. and V.V.; validation, G.N., C.B., N.M. and V.V.; writing—original draft preparation, G.N., C.B., N.M., O.B. and V.V.; writing—review and editing, G.N., C.B., N.M., O.B. and V.V.; visualization, G.N., C.B. and N.M.; supervision, N.M.; funding acquisition, G.N., C.B. and N.M. All authors have read and agreed to the published version of the manuscript.

Funding: This project has received funding from the European Union’s Horizon 2020 research and innovation programme under grant agreement no. 871124 LASERLAB-EUROPE.

Data Availability Statement: Data is contained within the article.

Acknowledgments: During the preparation of this manuscript/study, the author(s) used ChatGPT (version 5.0) to assist with English language editing, specifically syntax and grammar corrections. The authors have reviewed and edited the output and take full responsibility for the content of this publication.

Conflicts of Interest: The authors declare no conflicts of interest.

Abbreviations

The following abbreviations are used in this manuscript:

PMMA	Poly(methyl methacrylate)
IOL	Intra Ocular Lens
OCT	Optical Coherence Tomography

SEM	Scanning Electron Microscope
FS	Femto second

References

1. Khairallah, M.; Kahloun, R.; Bourne, R.; Limburg, H.; Flaxman, S.R.; Jonas, J.B.; Keeffe, J.; Leasher, J.; Naidoo, K.; Pesudovs, K.; et al. Number of People Blind or Visually Impaired by Cataract Worldwide and in World Regions, 1990 to 2010. *Invest. Ophthalmol. Vis. Sci.* **2015**, *56*, 6762–6769. [CrossRef] [PubMed]
2. Davison, J.A.; Simpson, M.J. History and Development of the Apodized Diffractive Intraocular Lens. *J. Cataract Refract. Surg.* **2006**, *32*, 849–858. [CrossRef] [PubMed]
3. Khandelwal, S.S.; Jun, J.J.; Mak, S.; Booth, M.S.; Shekelle, P.G. Effectiveness of Multifocal and Monofocal Intraocular Lenses for Cataract Surgery and Lens Replacement: A Systematic Review and Meta-Analysis. *Graefes Arch. Clin. Exp. Ophthalmol.* **2019**, *257*, 863–875. [CrossRef]
4. Olson, R.J.; Werner, L.; Mamalis, N.; Cionni, R. New Intraocular Lens Technology. *Am. J. Ophthalmol.* **2005**, *140*, 709–716. [CrossRef]
5. Mol, I.E.; Van Dooren, B.T. Toric Intraocular Lenses for Correction of Astigmatism in Keratoconus and after Corneal Surgery. *Clin. Ophthalmol.* **2016**, *10*, 1153–1159. [CrossRef]
6. Ninos, G.; Vassiliades, P. Advancements in Wavefront Aberrometry: Precision Measurement and Applications in Auto-Refractive Technologies. *Res. Med. Eng. Sci.* **2024**, *11*, RMES.000755. [CrossRef]
7. Javitt, J.C.; Steinert, R.F. Cataract Extraction with Multifocal Intraocular Lens Implantation: A Multinational Clinical Trial Evaluating Clinical, Functional, and Quality-of-Life Outcomes. *Ophthalmology* **2000**, *107*, 2040–2048. [CrossRef]
8. Sen, H.N.; Sarikkola, A.U.; Uusitalo, R.J.; Laatikainen, L. Quality of Vision after AMO Array Multifocal Intraocular Lens Implantation. *J. Cataract Refract. Surg.* **2004**, *30*, 2483–2493. [CrossRef]
9. Braga-Mele, R.; Chang, D.; Dewey, S.; Foster, G.; Henderson, B.A. Multifocal Intraocular Lenses: Relative Indications and Contraindications for Implantation. *J. Cataract Refract. Surg.* **2014**, *40*, 313–322. [CrossRef]
10. Lane, S.S.; Morris, M.; Nordan, L.; Packer, M.; Tarantino, N.; Wallace, R.B. Multifocal Intraocular Lenses. *Ophthalmol. Clin. N. Am.* **2006**, *19*, 89–105. [CrossRef]
11. Efthimiopoulos, T.; Kiagias, H.; Christoulakis, S.; Merlemis, N. Bubble Creation and Collapse during Excimer Laser Ablation of Weak Absorbing Polymers. *Appl. Surf. Sci.* **2008**, *254*, 5626–5630. [CrossRef]
12. Tokarev, V.N.; Lopez, J.; Lazare, S.; Weisbuch, F. High-Aspect-Ratio Microdrilling of Polymers with UV Laser Ablation: Experiment with Analytical Model. *Appl. Phys. A* **2003**, *76*, 385–396. [CrossRef]
13. Sinani, A.; Palles, D.; Bacharis, C.; Kandyla, M.; Riziotis, C. Laser Processing of Intraocular Lenses. *Appl. Sci.* **2024**, *14*, 6071. [CrossRef]
14. Kudryashov, S.; Gulina, Y.; Danilov, P.; Smirnov, N.; Rimskaya, E.; Krasin, G.; Saraeva, I.; Shelygina, S.; Rupasov, A.; Pershin, K.; et al. Photo-Physical Mechanism of Near-IR Femtosecond Laser-Induced Refractive-Index Change in PMMA. *Opt. Lett.* **2025**, *50*, 129–132. [CrossRef]
15. Ndifon, I.N.; Dikandé, A.M. Dynamics of Femtosecond Lasers and Induced Plasma in Non-Kerr Nonlinear Transparent Materials. *AIP Adv.* **2024**, *14*, 055320. [CrossRef]
16. Serafetinides, A.A.; Makropoulou, M.; Fabrikesi, E.; Spyratou, E.; Bacharis, C.; Thomson, R.R.; Kar, A.K. Ultrashort Laser Ablation of PMMA and Intraocular Lenses. *Appl. Phys. A* **2008**, *93*, 111–116. [CrossRef]
17. Spyratou, E.; Makropoulou, M.; Tsoutsis, D.; Zoulinakis, G.; Bacharis, C.; Asproudis, I.; Serafetinides, A.A. Conical Structures on Acrylic Intraocular Lens (IOLs) Materials after 193-nm Excimer. *Mater. Sci. Appl.* **2012**, *3*, 414–424. [CrossRef]
18. Kareliotis, G.; Drakaki, E.; Bacharis, C.; Makropoulou, M.; Serafetinides, A.A. Laser–Intraocular Lenses Interaction. Aspects to Consider for In-Situ Vision Correction. *New Front. Ophthalmol.* **2020**, *6*, 1000250. [CrossRef]
19. Heberle, J.; Klampfl, F.; Alexeev, I.; Michael Schmidt, M. Ultrashort Pulse Laser Cutting of Intraocular Lens Polymers. *J. Laser Micro Nanoeng.* **2014**, *9*, 103–107. [CrossRef]
20. Le Phu, T.; Molinero, M.L.; Boussard-Plédel, C.; Le Coq, D.; Masselin, P. Femtosecond Laser Fabrication of Gradient Index Micro-Optics in Chalcogenide Glass. *Photonics* **2024**, *11*, 1076. [CrossRef]
21. Mamalis, N. Femtosecond Laser Corrects Power of Implanted IOL. *EyeNet Magazine AAO*, 28 October 2017. Available online: <https://www.aao.org/eyenet/article/femtosecond-laser-corrects-power-of-implanted-iol> (accessed on 25 June 2025).
22. Sola, D.; Cases, R. High-Repetition-Rate Femtosecond Laser Processing of Acrylic Intra-Ocular Lenses. *Polymers* **2020**, *12*, 242. [CrossRef]
23. Obilor, A.; Pacella, M.; Wilson, A. Micro-Texturing of Polymer Surfaces Using Lasers: A Review. *Int. J. Adv. Manuf. Technol.* **2022**, *120*, 103–135. [CrossRef]
24. Sfregola, F.A.; De Palo, R.; Gaudiuso, C.; Mezzapesa, F.P.; Patimisco, P.; Ancona, A.; Volpe, A. Influence of Working Parameters on Multi-Shot Femtosecond Laser Surface Ablation of Lithium Niobate. *Opt. Laser Technol.* **2024**, *177*, 111067. [CrossRef]

25. Maruo, S.; Nakamura, O.; Kawata, S. Three-Dimensional Microfabrication with Two-Photon-Absorbed Photopolymerization. *Opt. Lett.* **1997**, *22*, 132–134. [[CrossRef](#)]
26. Malinauskas, M.; Žukauskas, A.; Hasegawa, S. Ultrafast laser processing of materials: From science to industry. *Light Sci. Appl.* **2016**, *5*, e16133. [[CrossRef](#)]
27. Scully, P.J.; Jones, D.; Jaroszynski, D.A. Femtosecond Laser Irradiation of Polymethylmethacrylate with an Embedded Photochromic Molecule. *Appl. Phys. A* **2001**, *73*, 561–566. [[CrossRef](#)]
28. Chichkov, B.N.; Momma, C.; Nolte, S. Femtosecond, picosecond and nanosecond laser ablation of solids. *Appl. Phys. A* **1996**, *63*, 109–115. [[CrossRef](#)]
29. Gattass, R.R.; Mazur, E. Femtosecond Laser Micromachining in Transparent Materials. *Nat. Photonics* **2008**, *2*, 219–225. [[CrossRef](#)]
30. Philips, K.C.; Gandhi, H.H.; Mazur, E.; Sundaram, S.K. Ultrafast laser processing of materials: A review. *Adv. Opt. Photonics* **2015**, *7*, 684–712. [[CrossRef](#)]
31. Bonse, J.; Baudach, S.; Krüger, J. Femtosecond laser ablation of silicon—modification thresholds and morphology. *Appl. Phys. A* **2002**, *74*, 19–25. [[CrossRef](#)]
32. Tan, B.; Venkatakrishnan, K.; Tok, T. A Femtosecond Laser-Induced Periodical Surface Structure on Polymethyl Methacrylate. *J. Micromech. Microeng.* **2003**, *13*, 778. [[CrossRef](#)]
33. Bacharis, C.; Tsilikas, G.; Sianoudis, I.; Makropoulou, M.; Zoulinakis, G.; Serafetinides, A.A. Laser Induced Refractive Index Modification of Intraocular Lenses. *E-J. Sci. Technol.* **2018**, *13*, 89–96.

Disclaimer/Publisher’s Note: The statements, opinions and data contained in all publications are solely those of the individual author(s) and contributor(s) and not of MDPI and/or the editor(s). MDPI and/or the editor(s) disclaim responsibility for any injury to people or property resulting from any ideas, methods, instructions or products referred to in the content.